

Shape Selectivity Effects in the Hydroconversion of Perhydrophenanthrene over Bifunctional Catalysts

Larissa Brito, Gerhard D. Pirngruber, Javier Perez-Pellitero, Emmanuelle Guillon, Florian Albrieux, Johan A. Martens

▶ **To cite this version:**

Larissa Brito, Gerhard D. Pirngruber, Javier Perez-Pellitero, Emmanuelle Guillon, Florian Albrieux, et al.. Shape Selectivity Effects in the Hydroconversion of Perhydrophenanthrene over Bifunctional Catalysts. Catalysis Science & Technology, 2021, 11 (23), pp.7667-7682. 10.1039/D1CY01556G . hal-03562682

HAL Id: hal-03562682
https://ifp.hal.science/hal-03562682

Submitted on 9 Feb 2022

HAL is a multi-disciplinary open access archive for the deposit and dissemination of scientific research documents, whether they are published or not. The documents may come from teaching and research institutions in France or abroad, or from public or private research centers.

L'archive ouverte pluridisciplinaire **HAL**, est destinée au dépôt et à la diffusion de documents scientifiques de niveau recherche, publiés ou non, émanant des établissements d'enseignement et de recherche français ou étrangers, des laboratoires publics ou privés.



Distributed under a Creative Commons Attribution - NonCommercial 4.0 International License

Catalysis Science & Technology

ROYAL SOCIETY OF CHEMISTRY

PAPER

View Article Online
View Journal | View Issue

Open Access Article. Published on 21 October 2021. Downloaded on 2/2/2022 7:01:03 PM.
This article is licensed under a Creative Commons Attribution-NonCommercial 3.0 Unported Licence.





Cite this: *Catal. Sci. Technol.*, 2021, 11, 7667

Shape selectivity effects in the hydroconversion of perhydrophenanthrene over bifunctional catalysts†

Larissa Brito,[a] Gerhard D. Pirngruber, *[a] Javier Perez-Pellitero,[a] Emmanuelle Guillon,[a] Florian Albrieux[a] and Johan A. Martens [b]

Received 25th August 2021,
Accepted 16th October 2021

DOI: 10.1039/d1cy01556g

rsc.li/catalysis

Hydroconversion of perhydrophenanthrene was performed over Pt/Beta and Pt/ASA bifunctional catalysts and compared to results obtained on the Pt/USY zeolite catalyst, under the same operating conditions. Perhydrophenanthrene resulted from the hydrogenation of the parent aromatic, phenanthrene, on a Pt/alumina pre-catalyst. All three bifunctional catalysts followed the general reaction pathway observed previously, *i.e.* isomerization of perhydrophenanthrene by ring-shift and ring-contraction, followed either by the formation of alkyladamantanes or by ring-opening. The ring opening products cracked to smaller naphthenes. Yet, the intermediates of this general reaction network differed very clearly from one catalyst to another. These shape selectivity effects could be explained by GCMC simulations of the adsorption selectivities of different intermediates. Bulky intermediates were preferentially adsorbed on USY zeolites, whereas Beta zeolites adsorbed preferentially linear structures. The product distribution on Beta zeolites was explained through the formation of a central ring-opening intermediate which cracked rapidly to C_7 naphthenes. USY-based catalysts were the most active among the solids tested, while Beta zeolites were slightly more selective to generate cracked products.

1. Introduction

In petroleum refining, hydrocracking plays an important role in upgrading heavy oil fractions, such as vacuum gas oil (VGO), to more valuable fractions, such as middle distillates.[1–4] Hydrocracking employs bifunctional catalysts, which comprise acid and metal functions. In order to process heavy fractions such as VGO, large-pore catalysts must be employed to avoid diffusional limitations.[5–8] Zeolites and amorphous silica–alumina (ASA) are commonly used in hydrocracking units as the acid function of bifunctional catalysts.[9–12] The acid function works in synergy with a hydrogenating component, such as Pt or promoted MoS_2. The latter becomes more active than Pt if the environment contains high H_2S concentrations.[13–15]

VGO fractions are rich in cyclic molecules, such as naphthenes and aromatics.[16] Hydroconversion of small monocyclic naphthenes has been well described in the literature,[17–21] as well as the reaction pathways of alkanes.[22–31] The knowledge of reaction routes involved in the conversion of heavy and/or polycyclic naphthenes containing more than two cycles is scarcer.[11,32–38] In a preceding study, we established hydroisomerization and hydrocracking pathways of perhydrophenanthrene (PHP), a 3-cycle naphthene, over a bifunctional Pt/USY catalyst.[39] The model molecule was first isomerized to ring-shift and ring-contraction compounds. These isomers generated ring-opening products or went through further isomerization to produce alkyladamantanes. The latter are very stable molecules and resisted hydrocracking. The ring opening products underwent cracking, resulting in a broad distribution of carbon atoms.

Since PHP is a rather bulky reactant, we can expect shape selectivity effects to play a role in its conversion. It is, therefore, important to analyze how the reactivity depends on the pore size and structure. Indeed, previous work by Leite *et al.* demonstrated that the reaction pathway over zeolite Beta differed from the one over USY. Moreover, large pore sizes (mesopores in USY and silica–alumina) favored isomerization over cracking products.[40,41]

The very high resolutive power of GCxGC analysis that we have developed in our previous work allows us to push Leite's preliminary analysis further. In this paper we, therefore, present a detailed analysis of the reaction pathways of the hydroconversion of PHP over Pt/USY, Pt/Beta and Pt/ASA

[a] *Rond Point de l'échangeur de Solaize, IFP Energies Nouvelles, BP-3, 69360 Solaize, France. E-mail: gerhard.pirngruber@ifpen.fr*
[b] *Center for Surface Chemistry and Catalysis, KU Leuven, Celestijnenlaan 200F, 3001 Leuven, Belgium*

† Electronic supplementary information (ESI) available. See DOI: 10.1039/d1cy01556g

Open Access Article. Published on 21 October 2021. Downloaded on 2/2/2022 7:01:03 PM.
This article is licensed under a Creative Commons Attribution-NonCommercial 3.0 Unported Licence.

(amorphous silica–alumina) bifunctional catalysts. We identify the nature of reaction intermediates and of cracked products generated on each solid and relate the differences to shape selective effects. Monte Carlo simulations show that these shape selectivity effects can be attributed to different adsorption selectivities of the intermediates in the FAU and BEA topologies. We also address the question whether the formation of adamantanes is limited to the mesopores/external surface of zeolites or whether it can occur in the micropores of large-pore zeolites.

2. Materials and methods

2.1. Preparation and characterization of catalysts

Ultra-stable-Y (CBV720) and Beta (CP814e) zeolites were provided by Zeolyst. The powder was mixed with an alumina binder (Pural SB3), furnished by Sasol, and extruded, according to a protocol described elsewhere.[39,42] Zeolite loading corresponded to 1 or 3 wt% of the dried support. The low zeolite loadings were chosen in order to obtain activity values of the same order of magnitude as a silica–alumina catalyst. Amorphous silica–alumina (Siralox 30) was supplied by Sasol in its extrudate form. All supports were calcined at 600 °C, under an air flow of 1.5 NL h^{-1} $g_{support}^{-1}$. For a good control of the hydrodynamics in the reactor, the extrudates were sorted to a length from 3 to 6 mm. The Pt precursor (H_2PtCl_6 from Sigma-Aldrich) was deposited on the extrudates by incipient wetness impregnation, in the presence of hydrochloric acid as a competitor. Further details on the preparation of catalysts may be found in previous work.[39] Pt-Based catalysts were calcined at 520 °C for 2 h, under an air flow of 1 NL h^{-1} $g_{catalyst}^{-1}$. A 0.8 wt% Pt/Al_2O_3 catalyst was prepared using the same procedure and used as a pure hydrogenation catalyst.

The content of Pt in the catalysts was determined with X-ray fluorescence and the dispersion of Pt was measured by H_2–O_2 chemisorption. Pt particles were considered to be spherical for the calculation of their size. The concentration of Brønsted acid sites (BAS) of the parent zeolites was determined from pyridine adsorption followed by FTIR. The concentration of BAS in USY and BETA parent zeolites corresponded to *ca.* 200 and 220 μmol g^{-1}, respectively.[43] The BAS concentration of the final catalysts was estimated by a rule of proportionality, considering that extrusion did not affect the acidity of the shaped support.[44] The BAS acidity of ASA was below the limit of reliable quantification. We also tested the H/D exchange method proposed by Hensen and co-workers,[45] but ASA did not show any O–D bands which could be attributable to strongly acidic sites when exposed to C_6D_6 at room temperature. The properties are summarized in Table 1.

2.2. Catalytic tests

A downflow fixed-bed reactor was used to perform catalytic tests at 280 or 300 °C and 60 bar. The reactor was loaded with a stacking of 2 g of Pt/Al_2O_3 and 2 g of bifunctional catalyst. Prior to the tests, the solids were reduced *in situ*, at 450 °C for 2 h under a H_2 flow of 1 NL h^{-1} $g_{catalyst}^{-1}$. The feedstock was composed of 3 wt% phenanthrene (Alfa Aesar) diluted in 97 wt% *n*-heptane (AnalaR Normapur). *N*-Heptane was chosen as a solvent because it does not crack readily. A high hydrogen to hydrocarbon molar ratio of 7 mol mol^{-1} was applied for all the tests and ensured the total hydrogenation of the parent aromatic to the naphthenic molecule over the Pt/Al_2O_3 pre-catalyst. This ratio also avoided catalyst deactivation throughout the tests. Different conversion degrees of PHP were obtained by changing the feed flow entering the reactor. Gas phase reaction products were analyzed online with a GC-FID apparatus (Varian). Liquid phase reaction products were collected for offline identification and quantification, with GCxGC-FID/MS. Further details on the analysis of reaction products are available elsewhere.[39]

The molar flow of a carbon number fraction (N_i) along with catalytic descriptors comprising the conversion of perhydrophenanthrene (X), yield of reaction products (Y_i) and distribution of a given product i within a family J ($D_{i,J}$) was calculated according to eqn (1)–(4).

$$N_i = \frac{(\mathrm{wt\%})_i \times F_\mathrm{m} \times c_i}{(100 \times M_i)} \quad (1)$$

F_m is the mass flow of the feedstock and $(\mathrm{wt\%})_i$, c_i and M_i the mass fraction, the number of carbons and the molar mass of the component i at the outlet, respectively.

$$X = 1 - \frac{N_{\mathrm{PHP,out}}}{\sum_{i=1}^{i=14} N_{i,\mathrm{out}}} \quad (2)$$

$$Y_i = \frac{N_i}{\sum_{i=1}^{i=14} N_{i,\mathrm{out}}} \quad (3)$$

Table 1 Properties of Pt-loaded zeolite and amorphous catalysts determined by X-ray fluorescence, H_2–O_2 chemisorption and pyridine adsorption monitored with FTIR

Type of support	Zeolite content in binder (wt%)	Pt loading (wt%)	Pt dispersion (%)	Pt particle size (nm)	n_{Pt} (μmol g^{-1})	BAS (μmol g^{-1})
USY (CBV720)	1	0.60	48	2.3	9.0	2.0
Beta (CP814e)	1	0.65	45	2.5	9.0	2.2
USY (CBV720)	3	0.66	89	1.3	18.8	6.0
Beta (CP814e)	3	0.69	85	1.3	15.8	6.6
ASA (Siralox 30)	—	0.60	84	1.3	15.8	n.d.

 This journal is © The Royal Society of Chemistry 2021

Open Access Article. Published on 21 October 2021. Downloaded on 2/2/2022 7:01:03 PM.
This article is licensed under a Creative Commons Attribution-NonCommercial 3.0 Unported Licence.

$$D_{i,J} = \frac{N_{i\in J}}{\sum N_{i\in J}} \quad (4)$$

For calculating the conversion and yields, material balances were generally expressed on a carbon mole basis. For comparing the yield/selectivity/distribution of the different cracked products, however, it was more convenient to use moles instead of carbon moles. When distributions are shown, the percentages refer to the relative abundance of a given compound within a family.

The contact time was expressed as 1/WHSV, and WHSV was defined as the liquid mass flow divided by the mass of the catalyst.

2.3. Grand Canonical Monte Carlo (GCMC) simulations

Grand Canonical Monte Carlo simulations combined with a bias scheme for the insertion of the center of mass of the guest molecules were performed at 280 °C to calculate the adsorbed amounts and selectivities of the different mixtures of hydrocarbons in both zeolites Beta and faujasite. The structure was represented by a 4 × 4 × 2 replication of the purely siliceous unit cell of the A polymorph of *BEA (taken from the IZA database[46]). The same strategy was employed for the faujasite by implementing a 2 × 2 × 2 unit cell replication system. The simulations were performed using the code GIBBS 9.3.[47] The adsorbate molecules were described according to the anisotropic united atoms potential (AUA) for hydrocarbons,[48,49] while the description of the zeolite was based on a "Kiselev type" potential.[50] The adsorbed amounts were determined from production runs of at least 50 million Monte Carlo steps. Further details about the model parameters and methodologies are provided in the ESI.†

3. Results

3.1. Identification and quantification of reaction products with GCxGC-FID/MS

The reaction products resulting from hydroisomerization and hydrocracking of PHP over Pt/USY, Pt/Beta and Pt/ASA bifunctional catalysts were identified and quantified with a two-dimensional GC coupled to FID and MS detectors. The chromatograms at similar PHP conversion are illustrated in Fig. 1. The conversion of phenanthrene, the parent aromatic, to the tricyclic naphthene was complete under the operating conditions applied during the catalytic tests. The method to distinguish PHP stereoisomers, *i.e.* the reactant, from reaction products was described in ref. 39.

The reaction products were lumped into families, according to their number of carbon atoms and chemical similarity. The six stereoisomers of PHP, obtained over the pre-catalyst Pt/Al_2O_3, were considered as the reactants, which underwent hydroisomerization and hydrocracking over the zeolite or silica–alumina catalysts.

Isomerization products ($C_{14}H_{24}$) were then divided into substituted adamantanes and other skeletal PHP isomers (Fig. 2). Among the latter, two subgroups were distinguished: ring-shift (perhydroanthracene and methylperhydrophenalenes) and ring-contraction isomers (having one 5-ring). Ring-opening products (ROPs, $C_{14}H_{26}$) were compounds presenting the same number of carbon atoms as PHP, but only two naphthenic cycles. Ring-opening of two out of three cycles of PHP was not observed among the reaction products.

Finally, cracked products comprised all the molecules with less than 14 carbon atoms and were mainly constituted of naphthenes.

3.2. Hydroconversion of perhydrophenanthrene

The conversion of PHP over Pt/USY, Pt/Beta and Pt/ASA bifunctional catalysts, as a function of contact time at 280 °C, is depicted in Fig. 3. The catalysts containing 3 wt% of zeolite were the most active among the solids tested. Results obtained with 1 wt% zeolite loading are available in the ESI.† There was a fairly good proportionality between zeolite content and activity (*i.e.* similar conversion at the same "zeolite" residence time). USY-based catalysts gave higher PHP conversion than the Beta zeolite. The activity of Pt/ASA at 280 °C was very low compared to the zeolite catalysts. We, therefore, raised the temperature to 300 °C, in order to achieve a reasonable range of PHP conversions (30 to 45%, see the ESI†). In the rest of the manuscript, the 300 °C data will be presented for ASA and compared with the zeolite data at 280 °C.

The yield of isomerization, ROP and cracking products (on a carbon molar basis) over Pt/USY, Pt/Beta and Pt/ASA catalysts is illustrated in Fig. 4. Isomerization products comprised skeletal PHP isomers and alkyladamantanes. Isomerization was the predominant reaction at low conversion. Over Pt/USY, a maximum yield of isomerization of *ca.* 43% was obtained at 68% conversion. Pt/Beta and Pt/ASA followed a similar profile, but the yield of isomerization products over zeolite Beta was slightly lower.

Ring-opening and cracking products were clearly secondary products. The ROP yield was quite low and reached a maximum at ~80% conversion. The yield of cracked products increased strongly above 40% PHP conversion. For the Pt/ASA catalyst, the contribution of cracking was very low. At medium conversion, Beta zeolites were slightly more selective to cracking products than USY and ASA, which goes in hand with the lower yield of isomerization products of Beta.

The distribution of PHP isomers, represented by skeletal isomers and alkyladamantanes, over Pt/USY, Pt/Beta and Pt/ASA bifunctional catalysts is revealed in Fig. 5. The proportion of alkyladamantanes increased with PHP conversion, whereas the proportion of skeletal PHP isomers decreased. Among the solids tested, USY zeolite seemed to be the most suitable for alkyladamantane production, in particular at high conversions. ASA-based catalysts were the

Open Access Article. Published on 21 October 2021. Downloaded on 2/2/2022 7:01:03 PM.
This article is licensed under a Creative Commons Attribution-NonCommercial 3.0 Unported Licence.

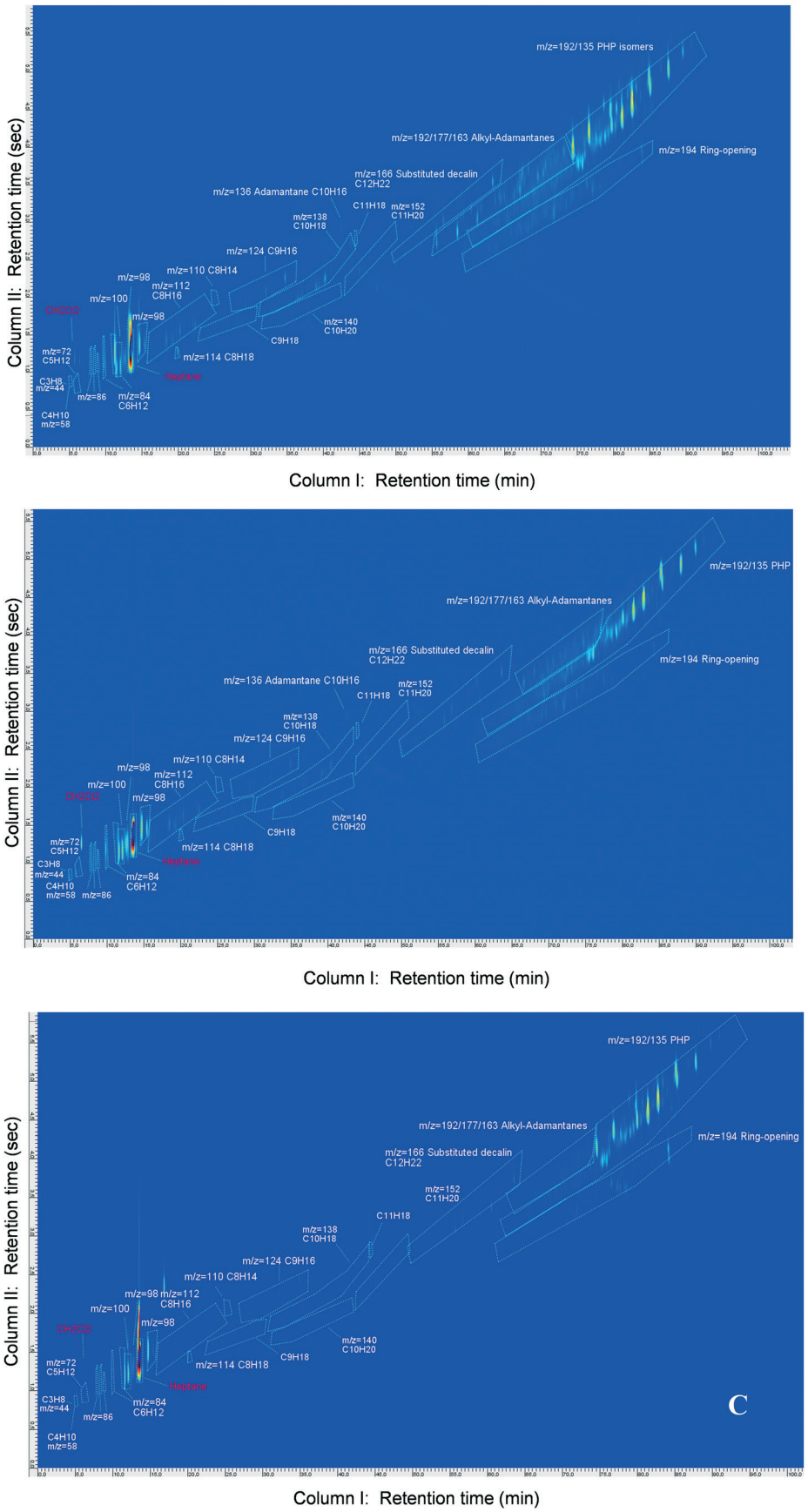


Fig. 1 GCxGC-FID analysis of reaction products from hydroconversion of perhydrophenanthrene obtained over A) Pt/USY zeolite catalyst at 48% conversion, B) Pt/Beta zeolite catalyst at 45% conversion, and C) Pt/ASA catalyst at 45% conversion.

 This journal is © The Royal Society of Chemistry 2021

Open Access Article. Published on 21 October 2021. Downloaded on 2/2/2022 7:01:03 PM.
This article is licensed under a Creative Commons Attribution-NonCommercial 3.0 Unported Licence.

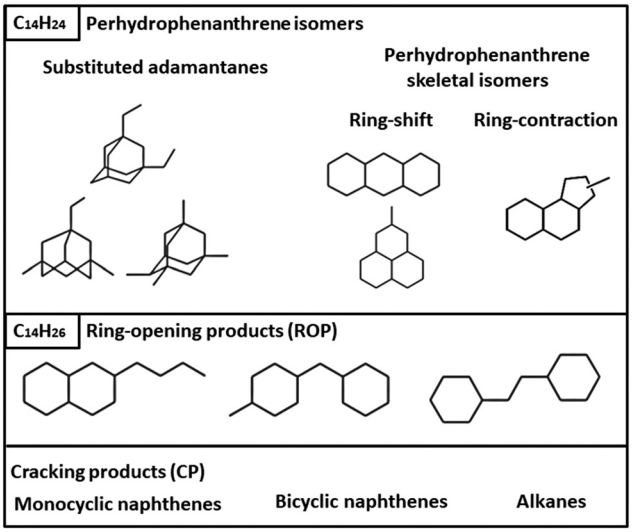


Fig. 2 Families and typical examples of molecules in the reaction products of hydroconversion of perhydrophenanthrene over Pt/USY, Pt/Beta and Pt/ASA bifunctional catalysts.

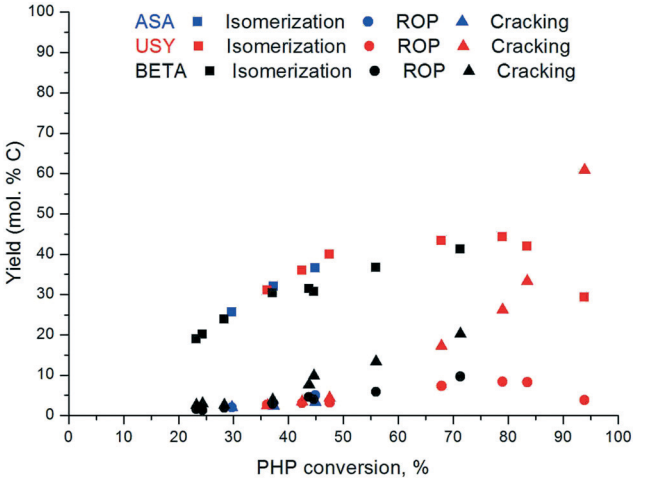


Fig. 4 Yield of isomerization, ring-opening and cracked products as a function of PHP conversion over Pt/USY and Pt/Beta at 280 °C and the Pt/ASA bifunctional catalyst at 300 °C.

least selective towards the formation of substituted adamantanes.

The distribution of skeletal PHP isomers over Pt/USY, Pt/Beta and Pt/ASA bifunctional catalysts at about 45% conversion is depicted in Fig. 6. We point out that structure **I4**, corresponding to a ring-contraction product of PHP, was completely absent on zeolite Beta. In contrast, this molecule was the major intermediate on USY zeolite and ASA at this conversion. This difference between USY and Beta had already been reported by Leite.[41] Structure **I1**, a ring-shift isomer of PHP (perhydroanthracene, PHA), was strongly favored over Pt/Beta at this conversion level, in comparison to the other catalysts. Precursors of alkyladamantanes, characterized by methylperhydrophenalenes (**I3**), were more abundant over Beta and ASA catalysts than over USY. Finally, spiro-type compounds, like isomer **I2**, were hardly detected over USY zeolites, but formed to a small extent over Beta and ASA based catalysts. At this conversion, the unknown fraction accounted for 20% of the distribution.

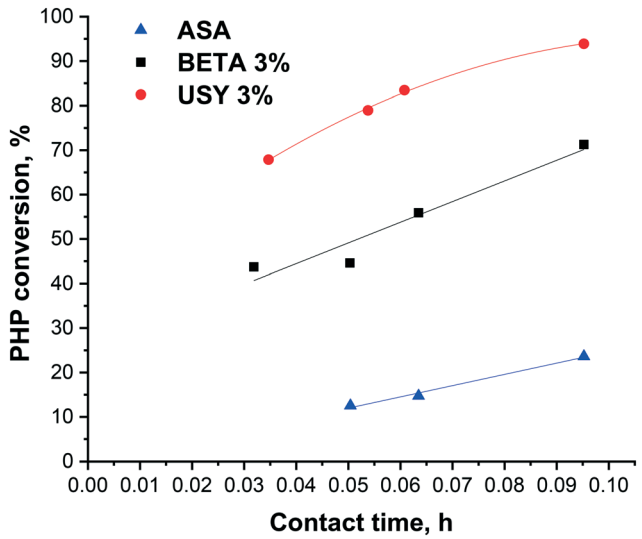


Fig. 3 Evolution of PHP conversion with contact time at 280 °C, on Pt/USY and Pt/Beta catalysts with 3 wt% zeolite in the alumina binder, and the Pt/ASA bifunctional catalyst.

The distribution of substituted adamantanes over Pt/USY, Pt/Beta and Pt/ASA catalysts at similar conversion is presented in Fig. 7. USY zeolite formed preferentially multibranched isomers, such as tetramethyladamantanes (**A1**), the thermodynamically most stable substituted adamantane,[51] and dimethyl-ethyladamantanes (**A3**). Zeolite Beta produced mainly isomers **A1** and **A2** (diethyladamantanes). Methylpropyladamantanes (**A4**), in addition to isomers **A3** and **A1**, were the dominating isomers over ASA. The unknown fraction accounted for about 20% of the distribution of alkyladamantanes on each solid tested.

Ring-opening products were represented by molecules presenting different degrees of branching, resulting from the opening of the external or central cycle of the model molecule and ring-contraction intermediates (Fig. 8). At ~45% PHP conversion, USY zeolites produced preferentially structures **R5**, **R1** (opening of the central cycle of PHP) and **R6**, **R7** (opening of the external cycle of PHP). Beta zeolites mainly generated structures **R1**, **R4** (cyclopentyl-cyclohexane structures) and **R6**. ASA catalysts produced mostly **R3** and **R6** intermediates, corresponding to the opening of the central and external cycle of PHP, respectively. The unknown fraction varied from 10% to 25% of the distribution.

The selectivity to cracked products resulting from hydroconversion of PHP over Pt/USY, Pt/Beta and Pt/ASA bifunctional catalysts is illustrated in Fig. 9. At 37% conversion, a predominant cracking to C_7 compounds was observed over the three catalysts, followed by the production

Open Access Article. Published on 21 October 2021. Downloaded on 2/2/2022 7:01:03 PM.
This article is licensed under a Creative Commons Attribution-NonCommercial 3.0 Unported Licence.

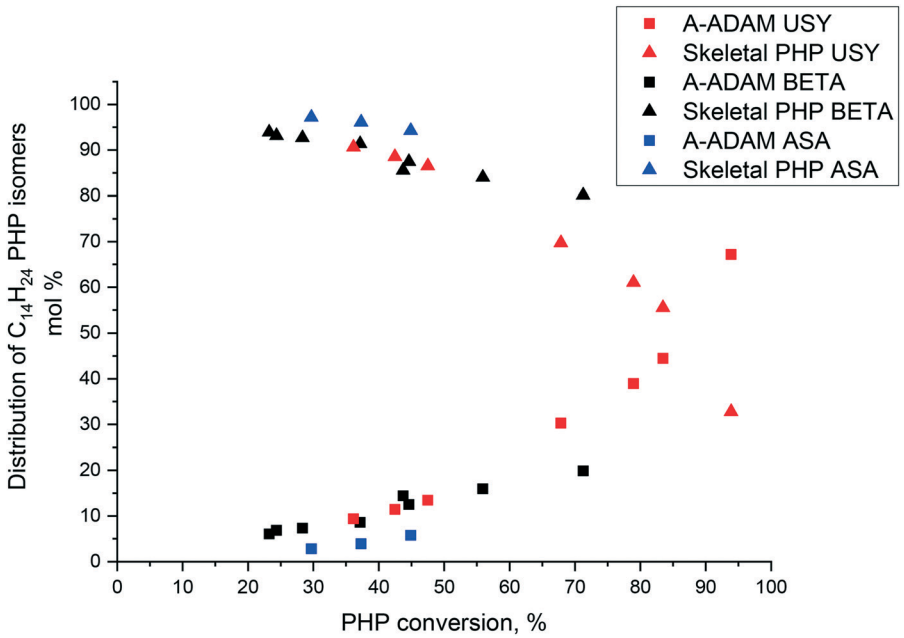


Fig. 5 Distribution of $C_{14}H_{24}$ reaction products from hydrocracking of PHP over Pt/USY, Pt/Beta and Pt/ASA bifunctional catalysts as a function of PHP conversion. Skeletal PHP isomers (▲), alkyladamantanes (■).

of C_{12}. Note that the production of C_{12} was not accompanied by the formation of light components, such as methane and ethane. Cracking to C_{12} molecules has been discussed in a previous work,[39] where reaction pathways leading to such products were understood as a contribution of disproportionation and addition–cracking reactions. When the conversion increased, USY catalysts gave a broader distribution of carbon atoms as cracked products, while over zeolite Beta and ASA a central cracking of PHP to C_7 molecules remained predominant. The main other cracking products were C_6 and C_8 compounds (formed in equimolar amounts), as well as C_4 (mainly isobutane) and C_{10} molecules.

Most of the cracked products were naphthenes (>80%). Iso-alkanes were minor products (less than 20% of the cracking products) and only very small amounts of *n*-alkanes were formed. The main alkane product was isobutane. The proportion of alkanes in the cracking products did not change much as a function of conversion. It is worth mentioning that C_7 isoalkanes were not counted in the distribution of cracked products, since it was not possible to determine whether they resulted from hydrocracking of the

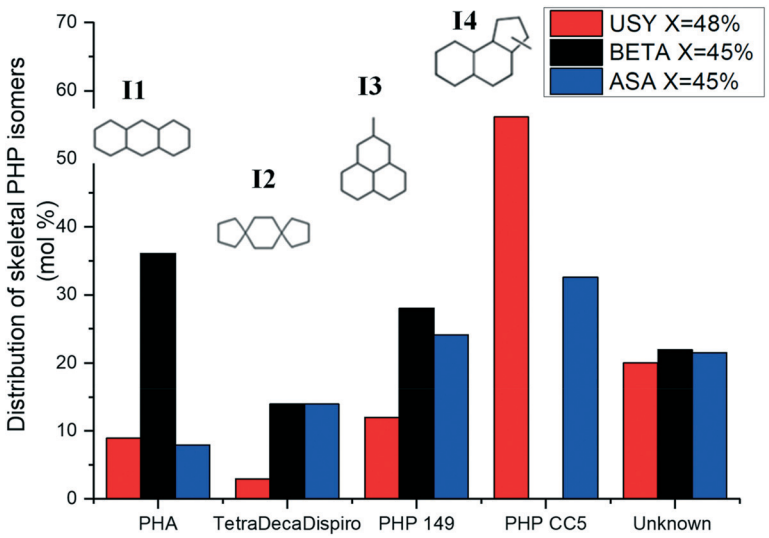


Fig. 6 Distribution of skeletal isomers of PHP (excluding substituted adamantanes) at isoconversion over Pt/USY, Pt/Beta and Pt/ASA bifunctional catalysts. PHP 149 stands for methylperhydrophenalene. PHP CC5 represents a skeletal PHP isomer containing a C_5-ring.

 This journal is © The Royal Society of Chemistry 2021

Open Access Article. Published on 21 October 2021. Downloaded on 2/2/2022 7:01:03 PM.
This article is licensed under a Creative Commons Attribution-NonCommercial 3.0 Unported Licence.

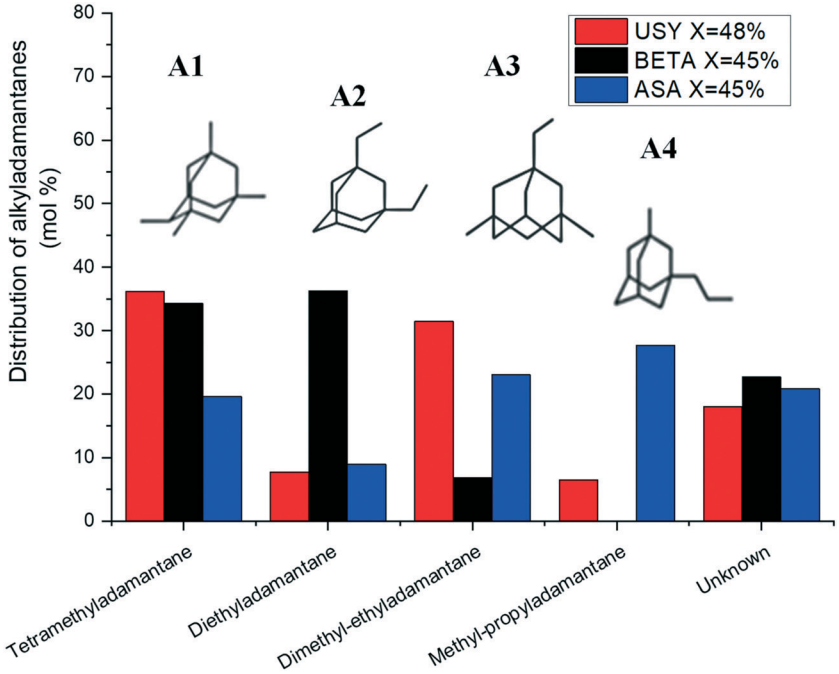


Fig. 7 Distribution of alkyladamantanes at isoconversion over Pt/USY, Pt/Beta and Pt/ASA bifunctional catalysts.

tricyclic model molecule or from isomerization of the solvent.

We examined the composition of the main cracking product, *i.e.* C_7 naphthenes, in more detail. The distribution of C_7 naphthenes over Pt/USY, Pt/Beta and Pt/ASA is presented in Fig. 10. Over Beta zeolites and ASA, primary C_7 cyclic compounds were composed of methylcyclohexanes, whereas dimethylcyclopentanes seemed to be formed in a primary route over Pt/USY. The proportion of dimethylcyclopentanes increased with conversion over Pt/Beta and Pt/ASA catalysts. Over the three catalysts, ethylcylopentane was observed to a small extent within this subfamily. These results indicate that Beta zeolites and silica–alumina supports differ from USY catalysts not only in terms of carbon number distribution, but also with respect to the nature of primary products formed.

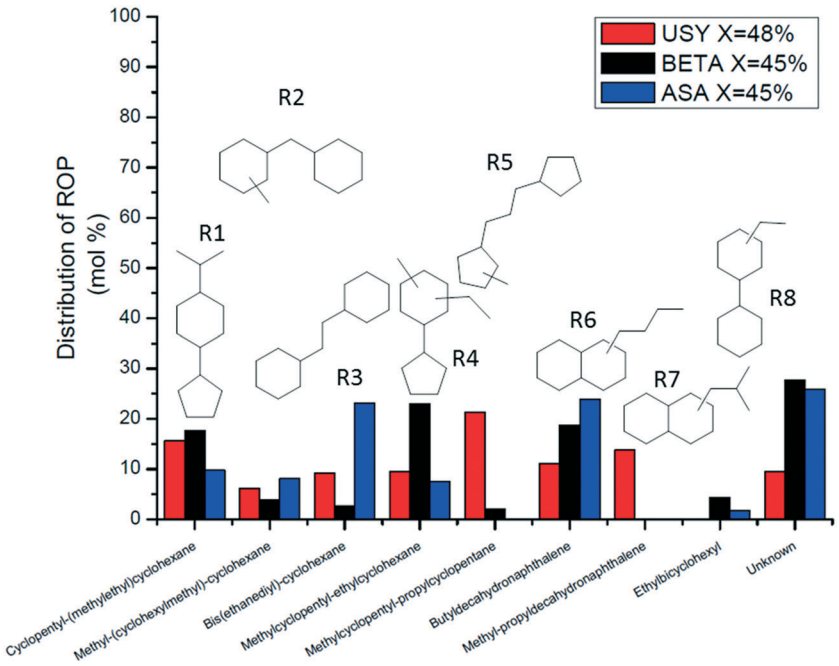


Fig. 8 Distribution of ring-opening products at isoconversion over Pt/USY, Pt/Beta and Pt/ASA bifunctional catalysts.

Open Access Article. Published on 21 October 2021. Downloaded on 2/2/2022 7:01:03 PM.
This article is licensed under a Creative Commons Attribution-NonCommercial 3.0 Unported Licence.

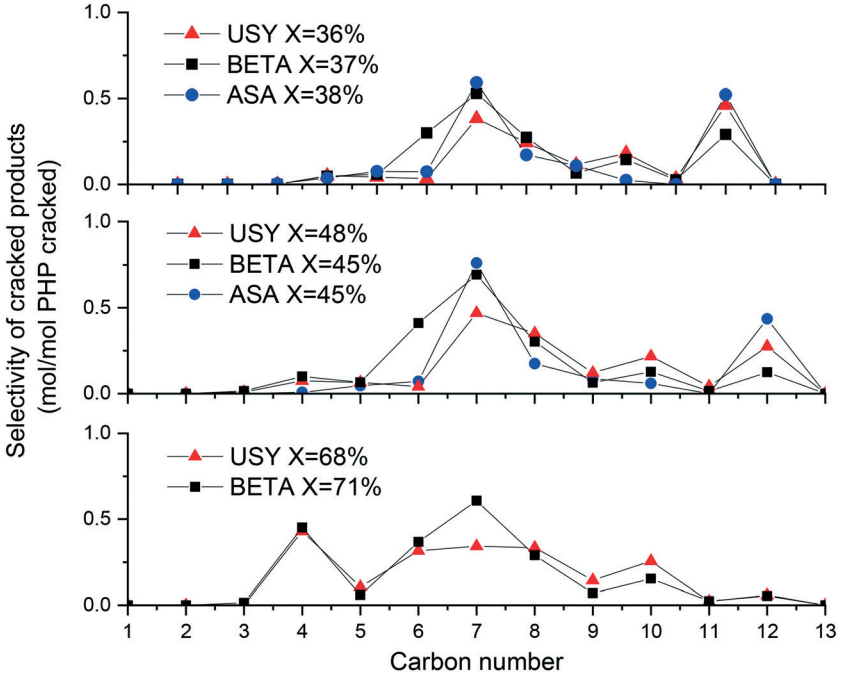


Fig. 9 Selectivity to cracked products according to the number of carbon atoms at similar conversion of PHP over Pt/USY, Pt/Beta and Pt/ASA bifunctional catalysts.

The detailed composition of each family of cracked products will not be presented herein, since the results are similar to the ones reported in our previous work regarding PHP conversion on Pt/USY.[39] C_6 and C_8 reaction products were mainly dimethylcyclopentanes and ethylcyclohexanes, while C_{10} structures were identified as decalin (decahydronaphthalene) and its isomers.

3.3. Molecular simulation

Fig. 6 and 8 show that the distribution of PHP isomers and of ring opening products is quite different on the three catalysts, *i.e.* we observe shape selectivity. Shape selectivity is often related to the fact that one isomer is preferentially adsorbed over another in a given zeolite.[52,53] In order to

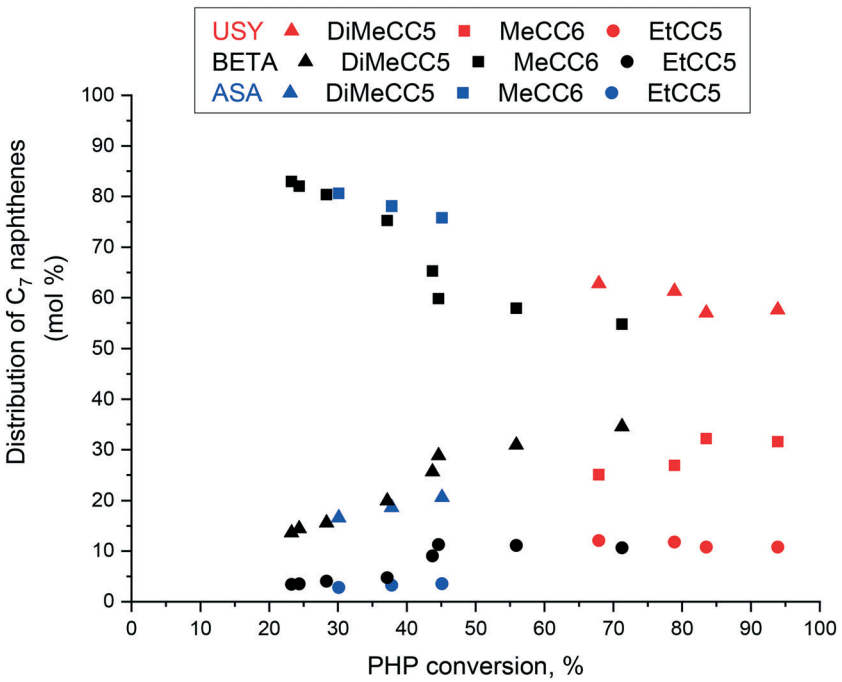


Fig. 10 Distribution of C_7 naphthenes as a function of PHP conversion over Pt/USY, Pt/Beta and Pt/ASA bifunctional catalysts. C_7 naphthenes were identified as dimethylcyclopentanes (triangles), methylcyclohexanes (squares) and ethylcyclopentanes (circles).

 This journal is © The Royal Society of Chemistry 2021

Open Access Article. Published on 21 October 2021. Downloaded on 2/2/2022 7:01:03 PM.
This article is licensed under a Creative Commons Attribution-NonCommercial 3.0 Unported Licence.

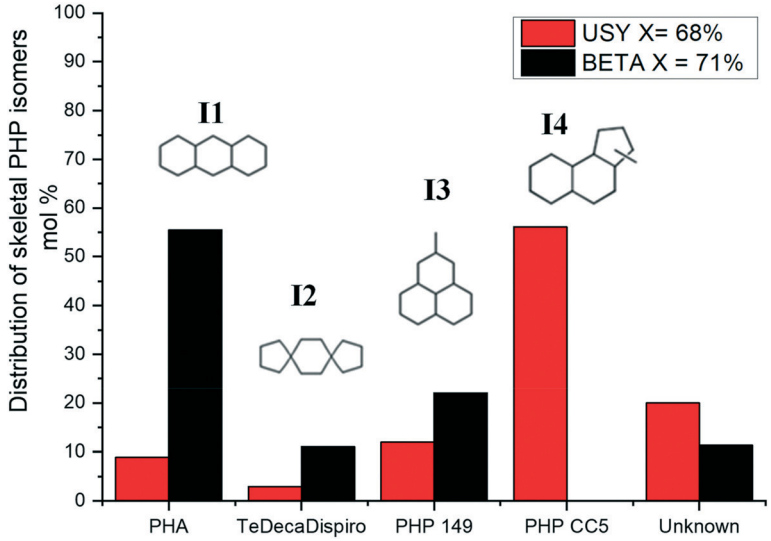


Fig. 11 Distribution of skeletal isomers of PHP (excluding substituted adamantanes) at isoconversion over Pt/USY and Pt/Beta bifunctional catalysts.

explore this hypothesis, a series of molecular simulations of the adsorption of selected intermediates were performed in the crystal structure of USY (FAU) and Beta (*BEA) zeolites. Taking into account the low polarity of the studied adsorbates and the main goal of the study (identifying the potential presence of shape selectivity), the purely siliceous forms of the mentioned structures were considered. The case of the amorphous silica–alumina was not evaluated with this method due to the uncertainty that could be introduced due to the lack of an accurate structural model as compared to the perfectly known zeolitic crystallographic frameworks.[54] For the molecular simulation study, we selected the most representative molecules found at *ca.* 70% PHP conversion.

As a first step, we investigated the competitive adsorption of the reactant PHP, skeletal PHP isomers and adamantanes on each zeolite. The choice of representative intermediates was made based on the distribution of skeletal PHP isomers and alkyladamantanes (Fig. 6, 7 and 11). Isomer **I4** (PHP CC5) was selectively formed over USY zeolites and ASA. In contrast, PHA isomers (**I1**) seemed to be favored over Beta zeolites, especially at high PHP conversion (Fig. 11). 1,3,5,7-Tetramethyladamantane was chosen as representative of the alkyladamantane family.

We, thus, carried out a simulation of the adsorption of an equimolar mixture of the reactant PHP, PHA (**I1**), the ring contraction isomer **I4** and 1,3,5,7-tetramethyladamantane, in the presence of *n*-heptane as a solvent. The chosen partial pressures were representative of the reaction conditions. The quantity of molecules adsorbed per volume is provided in Table 2. Clearly, both zeolites preferred the adsorption of PHP isomers **I1** and **I4** over the adsorption of alkyladamantanes. The adsorption of alkyladamantane was especially unfavorable (practically zero) on zeolite Beta.

Furthermore, adsorption of the ring-shift isomer PHA (**I1**) was more favored in zeolite BEA, in comparison to bulky molecules such as isomer **I4** (the ring contraction isomer of PHP). These trends were confirmed by carrying out simulations with a mixture containing only isomers **I1** and **I4** (Table 3). The **I1**/**I4** selectivity was *ca.* 3.2 for BEA, but only 1.06 for FAU. We can, therefore, assume that the preferential adsorption of PHA in BEA is partially responsible for the abundant formation of this intermediate in zeolite Beta.

Table 2 further demonstrates that the PHP reactant was less adsorbed in zeolite BEA than in the FAU structure.

4. Discussion

4.1. Global hydrocracking pathways

USY zeolite-based catalysts were the most active among the solids tested, followed by Beta and ASA catalysts. We note that a comparison of the same USY and Beta zeolites in the hydrocracking of *n*-hexadecane showed that zeolite Beta was more active than USY.[55] We presume that shape selectivity issues explain the inversion of activity ranking between USY

Table 2 Quantity of molecules adsorbed per volume as a function of zeolite topology. T = 280 °C, partial pressure of each component = 10 mbar, partial pressure of *n*-heptane = 8 bar

q_i (molecules per nm^3)					
Zeolite topology	PHP reactant	**A1** 1,3,5,7-tetramethyl-adamantane	**I4** (PHP CC5)	**I1** (PHA)	*n*-C_7
FAU	0.144	0.026	0.067	0.063	0.681
BEA	0.114	0.000	0.030	0.190	0.753

Open Access Article. Published on 21 October 2021. Downloaded on 2/2/2022 7:01:03 PM.
This article is licensed under a Creative Commons Attribution-NonCommercial 3.0 Unported Licence.

Table 3 Quantity of molecules adsorbed per volume as a function of zeolite topology. T = 280 °C, partial pressure of each component = 10 mbar

q_i (molecules per nm^3)			Selectivity
Zeolite topology	**I4** (PHP CC5)	**I1** (PHA)	**I1/I4**
FAU	0.310	0.328	1.06
BEA	0.215	0.684	3.18

and Beta. The molecular simulations showed that PHP isomers adsorbed much less in the pores of Beta zeolite than linear structures (Table 2). Hence, the access of the reactant to the acid sites in the micropores may be more restricted than in the faujasite structure.

All three catalysts globally followed the same reaction pathways (Fig. 4): ring-shift and ring-contraction PHP isomers were formed first as primary products. They either converted into alkyladamantanes or into ring-opening products. The latter underwent cracking. Cracking could only take place after the opening of at least one cycle of skeletal PHP isomers. The yield of ROPs was very low over USY, Beta and ASA, indicating that cracking occurred rapidly after the opening of a central or external cycle of PHP isomers. Alkyladamantanes, on the other hand, were not easily converted through hydrocracking to C_{10} adamantanes and isobutane, which is coherent with their high thermodynamic stability. Although this global scheme was common to all catalysts, the main members of each product family differed from one catalyst to another, as illustrated in Fig. 12. The reasons for these selectivity differences will be discussed in the following paragraphs.

4.2. Selectivity to adamantanes

We first take a closer look at the formation of adamantanes. As discussed before,[39] they are presumably formed from methylperhydrophenalene intermediates (**I3**).[51,56] Isomer **I3**, which is formed by ring-shift of PHP, was indeed observed over the three catalysts at all conversion levels. The selectivity to adamantane formation decreased in the order USY ≧ Beta > ASA. We will first discuss the difference between zeolite catalysts and ASA and then turn to the differences between USY and Beta zeolites.

Molecular simulations showed that alkyladamantanes were not easily adsorbed in the micropores of USY and Beta zeolites. Still, both zeolites produced significant amounts of alkyladamantanes, whereas ASA had a much lower selectivity to these products. The low adamantane selectivity of ASA is

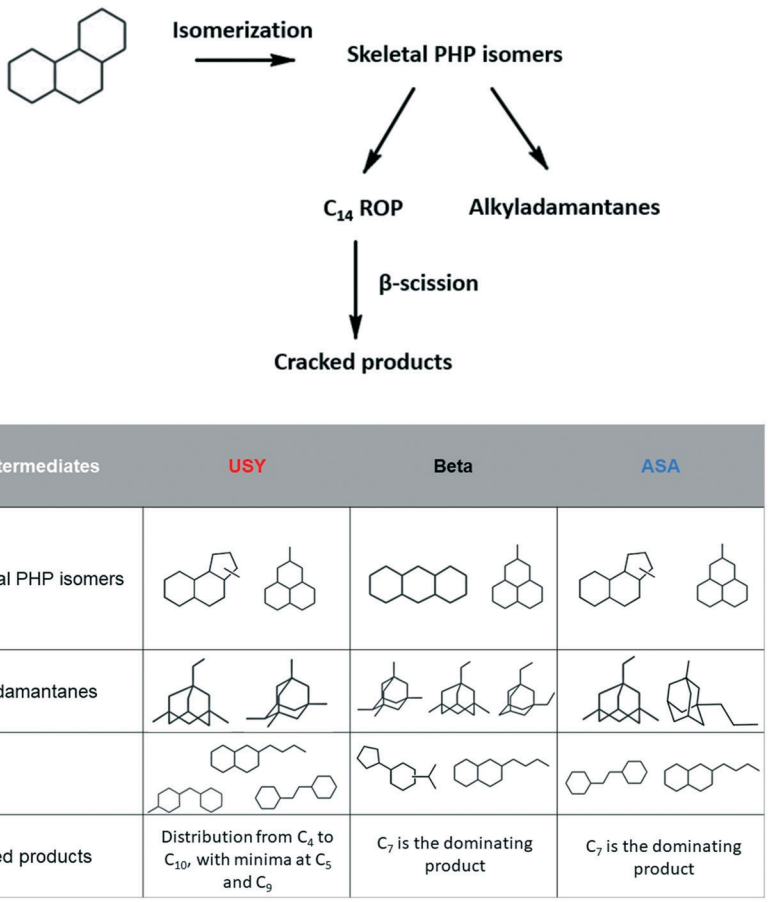


Fig. 12 Simplified reaction pathway for hydrocracking of perhydrophenanthrene over bifunctional Pt/Beta, Pt/USY zeolite catalysts and Pt/ASA catalyst. Main reaction intermediates obtained on each catalyst are illustrated.

 This journal is © The Royal Society of Chemistry 2021

Open Access Article. Published on 21 October 2021. Downloaded on 2/2/2022 7:01:03 PM.
This article is licensed under a Creative Commons Attribution-NonCommercial 3.0 Unported Licence.

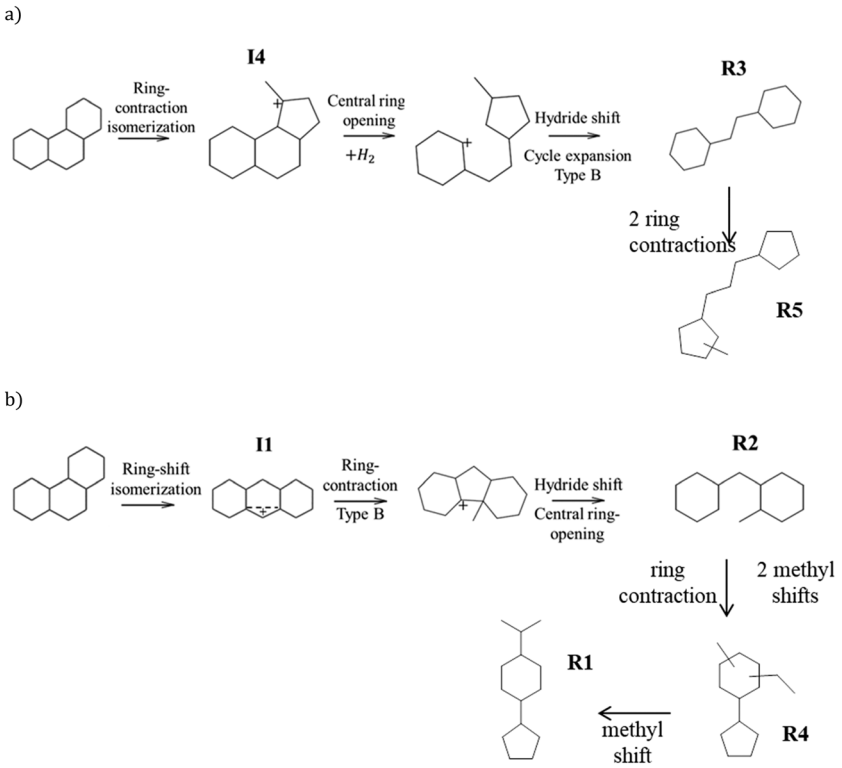


Fig. 13 Favorable ring opening pathways of the isomers a) **I4** and b) PHA (**I1**).

coherent with previous work:[37] the hydroconversion of fluorene over Pt/ASA produced only very little adamantane products. This result is somewhat surprising, since ASA may accommodate large molecules such as alkyladamantanes thanks to its large pore size (pore diameter of 70–80 Å). On the other hand, the tendency to generate alkyladamantanes in USY zeolites was previously attributed to the presence of supercages of 7.4 Å diameter, which corresponds to the van der Waals diameter of non-substituted adamantane,[37,57] but our simulations do not confirm that hypothesis of a good fit. We may infer from our results that a large pore size is not a sufficient criterion to form alkyladamantanes. The weak acid sites in amorphous silica–alumina are apparently not good catalysts for adamantane formation. Their production might be favored on the more strongly acidic zeolites, although the very bulky molecules cannot be easily accommodated in the zeolite micropores. We assume that alkyladamantane formation probably takes place in the pore mouths of the zeolites. The cavity effect of the pore mouth must make the difference compared to the silica–alumina, which does not exert any confinement effect.[58]

We note that Iglesia and co-workers[59] recently offered an alternative explanation for the different catalytic properties of zeolites and silica–alumina. They argued that the low selectivity of mesoporous silica–alumina catalysts to secondary/tertiary products (adamantanes and cracking products in our case) was due to the absence of diffusional constraints: primary intermediates were quickly hydrogenated before undergoing secondary reactions. Zeolites would favor the formation of secondary/tertiary products not because of higher acid strength, but because of a longer intracrystalline residence time of the primary intermediates in the micropores with high acid site density. In our case, we do not believe that this reasoning is applicable, since the formation of adamantanes presumably takes place in the pore mouths.

Let us now have a closer look at the adamantane formation on zeolite Beta. In spite of zero adsorption of adamantanes in BEA (according to the simulations), the selectivity to alkyladamantanes over Pt/Beta was non-zero, but still significantly lower than that of Pt/USY, at least at high conversion (Fig. 4 and 5). The higher alkyladamantane selectivity of USY *vs.* Beta is coherent with the literature. In a previous study, Rollmann and coworkers compared the effectiveness to convert perhydrofluorene,[57] a tricyclic naphthene, to trimethyladamantanes over Pt or Pd/USY and Pt or Pd/Beta zeolite catalysts. Under similar operating conditions, the yield of alkyladamantanes obtained over USY-based catalysts corresponded to 27%, whereas a yield of only 3% was acquired with Beta zeolites. Wang *et al.* studied the hydroconversion of fluorene on Pt-supported catalysts.[37] Higher yields of perhydrophenalene, precursors of alkyladamantanes, and propyladamantanes were obtained over the USY zeolite, in comparison to Beta. In our case, as shown in Fig. 6 and 11, methylperhydrophenalene (**I3**) was more abundant over Beta zeolites. It is likely that Beta zeolites did not easily convert these intermediates, hindering the further isomerization to alkyladamantanes.

Open Access Article. Published on 21 October 2021. Downloaded on 2/2/2022 7:01:03 PM.
This article is licensed under a Creative Commons Attribution-NonCommercial 3.0 Unported Licence.

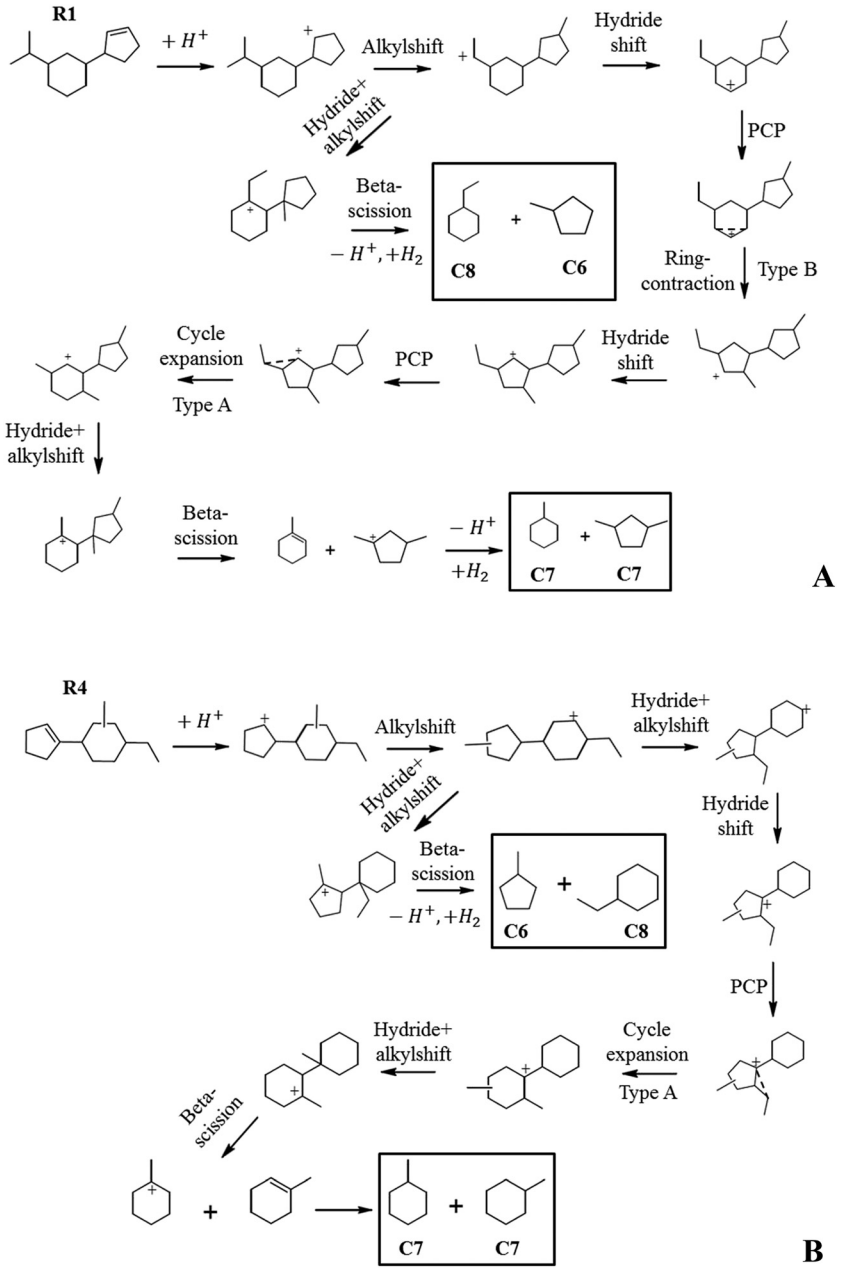


Fig. 14 A) Suggested hydrocracking pathway to C_7, C_6 and C_8 naphthenes resulting from hydroconversion of ring-opening intermediate **R1**. B) Suggested hydrocracking pathway to C_7, C_6 and C_8 naphthenes resulting from hydroconversion of ring-opening intermediate **R4**.

4.3. Isomerization and ring opening products

We now turn to the PHP isomers, which subsequently lead to the formation of ring opening products. In the Results section, we had already pointed out the remarkable result that ring-contraction PHP isomer **I4** (Fig. 6) was exclusively formed in the presence of USY and ASA. In accordance with Leite,[41] it was completely absent on zeolite Beta. Our molecular simulations showed that the adsorption of **I4** in zeolite Beta was quite unfavorable compared to more linear isomers. BEA adsorbed preferentially more linear structures, represented by PHA stereoisomers. It is clear that shape-selectivity impeded the production of bulky molecules on zeolite Beta, due to its more strained pore system. This different selectivity to PHP isomers in turn leads to different ring opening products.

As shown in Fig. 13, a very favorable ring opening pathway of **I4** leads to **R3**, which can subsequently rearrange to **R5** by very easy ring contraction reactions. An alternative favorable ring opening pathway of **I4** leads *via* β-scission in the external ring to butyl-decalin (**R6**), which can subsequently rearrange to **R7**. According to Fig. 8, the sum of **R3** + **R5** decreases in the order USY > ASA ≫ Beta. The sum of **R6** + **R7** follows the same order. We can deduce that the ring opening products,

 This journal is © The Royal Society of Chemistry 2021

Open Access Article. Published on 21 October 2021. Downloaded on 2/2/2022 7:01:03 PM.
This article is licensed under a Creative Commons Attribution-NonCommercial 3.0 Unported Licence.

which can be easily formed from **I4**, were less preferred in zeolite Beta.

Beta prefers the formation of PHA over **I4**; a favorable ring opening pathway of PHA (**I1**) leads to **R2** (Fig. 13b), which can subsequently rearranged to **R1** and **R4**. The sum of **R2** + **R1** + **R4** follows the order Beta > USY > ASA (Fig. 8). This trend can be linked to the preferential formation of PHA on zeolite Beta. We will discuss the implication on the distribution of cracking products in the next section.

4.4. Distribution of cracking products

In order to explain the distribution of cracked products, it is necessary to analyze the hydrocracking pathways of the major ROPs. The basis for this analysis was laid in our previous work on Pt/USY.[39]

Beta zeolites produced mainly structures **R1**, **R4** and **R6**, according to the distribution presented in Fig. 8. The cracking of butyldecalin (**R6**) to C_{10} naphthenes, represented by decalin and its isomers, and isobutane was observed at high PHP conversion. Yet, the major cracking products of zeolite Beta were not C_{10} and C_4, but C_7, followed by C_6 and C_8 (Fig. 9).

We tried to construct reaction pathways for the cracking of intermediates **R1** and **R4** to C_7 naphthenes (Fig. 14A and B). Several rearrangements, including a slow step of ring-contraction (type B isomerization), were necessary to achieve a configuration allowing fast beta-scission. In both cases, cracking leading to C_6 and C_8 was more easily obtained through exocyclic alkyl shifts, generating dimethylcyclopentanes and ethylcyclohexanes. We, therefore, presume that the cracking of **R1** and **R4** explains the formation of C_6 and C_8 naphthene products.

Preferential cracking to C_7 naphthenes over Beta zeolites can only be rationalized from the consumption of the **R2** intermediate, which is the favored ring opening product of PHA (Fig. 15). The distribution of ROPs (Fig. 8) shows that **R2** accounts for *ca.* 10% of the distribution at low PHP conversion, and its content decreases to virtually zero at high PHP conversion. **R2** can very easily crack to C_7 naphthenes by a fast tertiary–tertiary beta-scission, once the alkyl group has been shifted to a favorable position, as illustrated in Fig. 15 (we note that this pathway is more favorable than the routes leading to the C_7 isomers preferred on USY or to C_6 + C_8, which had been proposed in ref. 39). We presume that the **R2** intermediate is very quickly consumed by this very favorable cracking pathway, which explains its low abundance in the products. The pathway shown in Fig. 15 must be the main hydrocracking pathway over the Pt/Beta zeolite catalyst, since it can explain the exclusive formation of methylcyclohexane as the primary C_7 product on Beta zeolites (Fig. 10). Since ASA exhibits the same high selectivity to methylcyclohexane, this pathway must also play an important role in silica–alumina. The similarity in the product distribution of ASA and Beta reinforces the idea that a lot of catalysis on zeolite Beta may be going on in the pore mouth or on its outer surface.

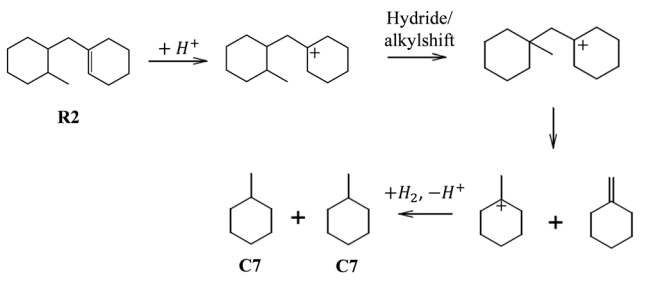


Fig. 15 Very favorable hydrocracking pathway of ring-opening product **R2** to C_7 naphthenes.

We note that the ROPs, which dominate in the product distribution, are not necessarily the ones which explain best the cracking pattern, because they may actually correspond to the most stable intermediates, *i.e.* those which crack least readily.

Finally, let us examine the question why USY does not as selectively crack to C_7 naphthenes as zeolite Beta. In USY, the preferred isomer was the ring-contraction isomer **I4**, which could favorably ring-open to **R3**. A cracking pathway from **R3** to C_7 products (involving dimethyl-cyclopentane, which is the main C_7 isomer on USY) had been proposed in ref. 39, but this pathway involves a type B isomerization step, shifting an alkyl group from the ring to the central alkyl chain. Moreover, the beta scission leads to a secondary carbenium ion. It will, thus, have a higher activation energy than the cracking pathway shown in Fig. 15 and will be less dominating compared to other possible reaction pathways leading to C_6 + C_8 naphthenes.

5. Conclusions

Hydroisomerization and hydrocracking of perhydrophenanthrene were performed over Pt/Beta and Pt/ASA bifunctional catalysts and compared to results obtained with the Pt/USY zeolite catalyst, under the same operating conditions. The common reaction pathway consists of converting the reactant into skeletal perhydrophenanthrene isomers, which are further transformed into substituted adamantanes or ring-opening products. The ring-opening products undergo rapid hydrocracking, whereas alkyladamantanes are stable.

USY-based catalysts were more active than Beta. Molecular simulations point out a weak adsorption of the PHP reactant on the pores of the BEA structure, indicating that the lower activity of Beta is linked to a limited access of the reactant to the micropores of zeolite Beta. ASA was by far the least active catalyst, due to its low acidity.

On top of the activity difference, shape selectivity effects were evidenced by comparing zeolites USY and Beta. The bulky ring-contraction isomers of PHP, which were dominating in USY, do not easily fit into the pores of zeolite Beta. The Beta structure prefers the adsorption of the ring-shift isomer perhydroanthracene (PHA). The preferential

Open Access Article. Published on 21 October 2021. Downloaded on 2/2/2022 7:01:03 PM.
This article is licensed under a Creative Commons Attribution-NonCommercial 3.0 Unported Licence.

adsorption of PHA can explain the very selective cracking to methyl-cyclohexane, which was observed over zeolite Beta: PHA offers a very favorable central ring opening pathway to methyl-(cyclohexylmethyl)-cyclohexane (**R2**), which can then readily crack to two methyl-cyclohexane molecules, leading to a peak at C_7 in the distribution of cracked products. For zeolite USY, on the other hand, the dominating ring-contraction isomer of PHP does not offer an equally favorable cracking pathway and, thus, leads to a broader distribution of cracking products.

Quite remarkably, zeolite Beta also produced significant amounts of alkyl-adamantanes (albeit less than USY), although these products absolutely do not fit into the pores of the BEA structure. Their formation is, therefore, attributed to pore mouth catalysis. ASA catalysts, on the other hand, were not very selective to alkyl-adamantanes, although the formation of these bulky molecules should be favored in the large pores of ASA. We tentatively attribute the difficulty to from adamantanes on ASA to the absence of confinement effects and/or of strong acid sites on the ASA surface.

With respect to PHP isomers, ring opening intermediates and cracking products, ASA showed a quite particular behavior. The main intermediates of the ASA catalyst resemble those of USY, but the distribution of cracking products is closer to Beta. The similarity in the distribution of cracking products on ASA suggests that a lot of catalysis on zeolite Beta may be going on in the pore mouth or on its outer surface.

From an application point of view, the results presented in this work will be a useful guide for catalyst selection in hydroconversion processes, especially when dealing with feeds with a high content of polyaromatic molecules. It will also help in improving the kinetic models of the hydrocracking process, where naphthene conversion is often treated in a very rudimentary manner, due to the lack of analytic information.[60,61]

Conflicts of interest

There are no conflicts to declare.

References

1 M. S. Rana, V. Samano, J. Ancheyta and J. A. I. Diaz, A review of recent advances on process technologies for upgrading of heavy oils and residua, *Fuel*, 2007, **86**, 1216–1231.
2 G. Valavarasu, M. Bhaskar and K. S. Balaraman, Mild hydrocracking - A review of the process, catalysts, reactions, kinetics, and advantages, *Pet. Sci. Technol.*, 2003, **21**, 1185–1205.
3 F. Bertoncini, A. Bonduelle, J. Francis and E. Guillon, in *Catalysis by Transition Metal Sulfides*, ed. H. Toulhoat and P. Raybaud, Technip, Paris, 2013, p. 609.
4 J. Scherzer and A. J. Gruia, *Hydrocracking science and technology*, M. Dekker, New York, 1996.
5 A. Corma, M. J. Diaz-Cabanas, C. Lopez and A. Martinez, Hydrocracking catalysts based on the new large-pore ITQ-21 zeolite for maximizing diesel products, *Stud. Surf. Sci. Catal.*, 2004, **154**, 2380–2386.
6 A. Chica and A. Corma, Comparison of large pore zeolites for n-octane hydroisomerization: Activity, selectivity and kinetic features, *Chem. Ing. Tech.*, 2007, **79**, 857–870.
7 T. F. Degnan, Jr, Applications of zeolites in petroleum refining, *Top. Catal.*, 2000, **13**, 349–356.
8 W. M. Zhang and P. G. Smirniotis, Effect of zeolite structure and acidity on the product selectivity and reaction mechanism for n-octane hydroisomerization and hydrocracking, *J. Catal.*, 1999, **182**, 400–416.
9 M. A. Ali, T. Tatsumi and T. Masuda, Development of heavy oil hydrocracking catalysts using amorphous silica-alumina and zeolites as catalyst supports, *Appl. Catal., A*, 2002, **233**, 77–90.
10 K. Sato, Y. Nishimura, K. Honna, N. Matsubayashi and H. Shimada, Role of HY Zeolite Mesopores in Hydrocracking of Heavy Oils, *J. Catal.*, 2001, **200**, 288–297.
11 H. W. Haynes, J. F. Parcher and N. E. Helmer, Hydrocracking Polycyclic Hydrocarbons over a Dual-Functional Zeolite (Faujasite)-Based Catalyst, *Ind. Eng. Chem. Process Des. Dev.*, 1983, **22**, 401.
12 V. Y. Pereyma, P. P. Dik, O. V. Klimov, S. V. Budukva, K. A. Leonova and A. S. Noskov, Hydrocracking of vacuum gas oil in the presence of catalysts NiMo/Al2O3–amorphous aluminosilicates and NiW/Al_2O_3–amorphous aluminosilicates, *Russ. J. Appl. Chem.*, 2015, **88**, 1969–1975.
13 C.-E. Hédoire, C. Louis, A. Davidson, M. Breysse, F. Maugé and M. Vrinat, Support effect in hydrotreating catalysts: hydrogenation properties of molybdenum sulfide supported on β-zeolites of various acidities, *J. Catal.*, 2003, **220**, 433–441.
14 N. Guernalec, T. Cseri, P. Raybaud, C. Geantet and M. Vrinat, Influence of H_2S on the hydrogenation activity of relevant transition metal sulfides, *Catal. Today*, 2004, **98**, 61–66.
15 N. Guernalec, C. Geantet, T. Cseri, M. Vrinat, H. Toulhoat and P. Raybaud, Compensation effect and volcano curve in toluene hydrogenation catalyzed by transition metal sulfides, *Dalton Trans.*, 2010, **39**, 8420–8422.
16 T. Dutriez, M. Courtiade, D. Thiébaut, H. Dulot, F. Bertoncini, J. Vial and M.-C. Hennion, High-temperature two-dimensional gas chromatography of hydrocarbons up to nC60 for analysis of vacuum gas oils, *J. Chromatogr. A*, 2009, **1216**, 2905–2912.
17 R. Nageswara Rao, N. You, S. Yoon, D. P. Upare, Y.-K. Park and C. W. Lee, Selective Ring Opening of Methylcyclopentane and Methylcyclohexane Over Iridium Bifunctional Catalysts Supported on Surface Modified γ-Al_2O_3, SiO_2 and Ultra Stable Y Zeolites, *Catal. Lett.*, 2011, **141**, 1047–1055.
18 H. Ziaei-Azad and A. Sayari, Bifunctional MCM-41 aluminosilicate supported Ir with adjusted metal and acid functionality for catalytic ring opening of 1,2-dimethylcyclohexane, *J. Catal.*, 2016, **344**, 729–740.

 This journal is © The Royal Society of Chemistry 2021

Open Access Article. Published on 21 October 2021. Downloaded on 2/2/2022 7:01:03 PM.
This article is licensed under a Creative Commons Attribution-NonCommercial 3.0 Unported Licence.

19 E. Gutierrez-Acebo, C. Leroux, C. Chizallet, Y. Schuurman and C. Bouchy, Metal/Acid Bifunctional Catalysis and Intimacy Criterion for Ethylcyclohexane Hydroconversion, *ACS Catal.*, 2018, **8**, 6035–6046.

20 S. A. D'Ippolito, C. Especel, L. Vivier, F. Epron and C. L. Pieck, Influence of the Brønsted acidity, SiO_2/Al_2O_3 ratio and Rh–Pd content on the ring opening. Part II. Selective ring opening of methylcyclohexane, *Appl. Catal., A*, 2014, **469**, 541–549.

21 J. Weitkamp and S. Ernst, in *Catalysis by Acids and Bases*, ed. B. Imelik, C. Naccache, G. Coudurier, Y. Ben Taarit and J. C. Vedrine, Elsevier, 1985, pp. 419–426.

22 F. Alvarez, G. Giannetto, M. Guisnet and G. Perot, Hydroisomerization and hydrocracking of n-Alkanes. 2. n-Heptane transformation on a Pt-dealuminated Y zeolite - comparison with a Pt-Y zeolite, *Appl. Catal.*, 1987, **34**, 353–365.

23 G. E. Giannetto, G. R. Perot and M. R. Guisnet, Hydroisomerization and hydrocracking of n-alkanes. 1. Ideal hydroisomerization PtHY catalysts, *Ind. Eng. Chem. Prod. Res. Dev.*, 1986, **25**, 481–490.

24 F. Alvarez, F. R. Ribeiro, G. Giannetto, F. Chevalier, G. Perot and M. Guisnet, in *Studies in Surface Science and Catalysis*, ed. A. Galarneau, F. Fajula, F. Di Renzo and J. Vedrine, Elsevier, 2001, pp. 1339–1348.

25 N. Batalha, L. Pinard, Y. Pouilloux and M. Guisnet, Bifunctional Hydrogenating/Acid Catalysis, *Catal. Lett.*, 2013, **143**, 587–591.

26 G. Burnens, C. Bouchy, E. Guillon and J. A. Martens, Hydrocracking reaction pathways of 2,6,10,14-tetramethylpentadecane model molecule on bifunctional silica-alumina and ultrastable Y zeolite catalysts, *J. Catal.*, 2011, **282**, 145–154.

27 M. C. Claude and J. A. Martens, Monomethyl-branching of long n-alkanes in the range from decane to tetracosane on Pt/H-ZSM-22 bifunctional catalyst, *J. Catal.*, 2000, **190**, 39–48.

28 J. Weitkamp, P. A. Jacobs and J. A. Martens, Isomerization and hydrocracking of C-9 through C-16 n-alkanes on Pt/HZSM-5 zeolite, *Appl. Catal.*, 1983, **8**, 123–141.

29 N. Batalha, L. Pinard, C. Bouchy, E. Guillon and M. Guisnet, n-Hexadecane hydroisomerization over Pt-HBEA catalysts. Quantification and effect of the intimacy between metal and protonic sites, *J. Catal.*, 2013, **307**, 122–131.

30 R. Kenmogne, A. Finiels, C. Cammarano, V. Hulea and F. Fajula, Hydroconversion of n-hexadecane over bifunctional microporous and mesoporous model catalysts. Influence of pore architecture on selectivity, *J. Catal.*, 2015, **329**, 348–354.

31 P. S. F. Mendes, F. M. Mota, J. M. Silva, M. F. Ribeiro, A. Daudin and C. Bouchy, A systematic study on mixtures of Pt/zeolite as hydroisomerization catalysts, *Catal. Sci. Technol.*, 2017, **7**, 1095–1107.

32 S.-U. Lee, Y.-J. Lee, J.-R. Kim, E.-S. Kim, T.-W. Kim, H. J. Kim, C.-U. Kim and S.-Y. Jeong, Selective ring opening of phenanthrene over NiW-supported mesoporous HY zeolite catalyst depending on their mesoporosity, *Mater. Res. Bull.*, 2017, **96**, 149–154.

33 L. Leite, E. Benazzi and N. Marchal-George, Hydrocracking of phenanthrene over bifunctional Pt catalysts, *Catal. Today*, 2001, **65**, 241–247.

34 A. T. Lapinas, M. T. Klein and B. C. Gates, Catalytic Hydrogenation and Hydrocracking of Fluorene: Reaction Pathways, Kinetics, and Mechanisms, *Ind. Eng. Chem. Res.*, 1991, **30**, 42–50.

35 T. Isoda, S. Maemoto, K. Kusakabe and S. Morooka, Hydrocracking of Pyrenes over a Nickel-Supported Y-Zeolite Catalyst and an Assessment of the Reaction Mechanism Based on MD Calculations, *Energy Fuels*, 1999, **13**, 617–623.

36 S. C. Korre, M. T. Klein and R. J. Quann, Polynuclear Aromatic Hydrocarbons Hydrogenation. 1. Experimental Reaction Pathways and Kinetics, *Ind. Eng. Chem. Res.*, 1995, **34**, 101–117.

37 L. Wang, Y. Chen, S. Jin, X. Chen and C. Liang, Selective Ring-Shift Isomerization in Hydroconversion of Fluorene over Supported Platinum Catalysts, *Energy Fuels*, 2016, **30**, 3403–3412.

38 W. Souverijns, R. Parton, J. A. Martens, G. F. Froment and P. A. Jacobs, Mechanism of the paring reaction of naphtenes, *Catal. Lett.*, 1996, **37**, 207–212.

39 L. Brito, G. D. Pirngruber, E. Guillon, F. Albrieux and J. A. Martens, Hydroconversion of perhydrophenanthrene over bifunctional Pt/H-USY zeolite catalyst, *ChemCatChem*, 2020, **12**, 3477–3488.

40 E. Benazzi, L. Leite, N. Marchal-George, H. Toulhoat and P. Raybaud, New insights into parameters controlling the selectivity in hydrocracking reactions, *J. Catal.*, 2003, **217**, 376–387.

41 L. Leite, *PhD thesis*, Université Paris VI, 2000.

42 P. S. F. Mendes, J. M. Silva, M. Filipa Ribeiro, A. Daudin and C. Bouchy, From powder to extrudate zeolite-based bifunctional hydroisomerization catalysts, *J. Ind. Eng. Chem.*, 2018, **62**, 72–83.

43 P. S. Mendes, G. Lapisardi, C. Bouchy, M. Rivallan, J. M. Silva and M. F. Ribeiro, Hydrogenating activity of Pt/zeolite catalysts focusing acid support and metal dispersion influence, *Appl. Catal., A*, 2015, **504**, 17–28.

44 Y. Bi, G. Xia, W. Huang and H. Nie, Hydroisomerization of long chain n-paraffins, *RSC Adv.*, 2015, **5**, 99201–99206.

45 D. G. Poduval, J. A. R. van Veen, M. S. Rigutto and E. J. M. Hensen, Brønsted acid sites of zeolitic strength in amorphous silica-alumina, *Chem. Commun.*, 2010, **46**, 3466–3468.

46 C. Baerlocher and L. B. McCusker, Database of Zeolite Structures, http://www.iza-structure.org/databases/.

47 P. Ungerer, B. Tavitian and A. Boutin, *Applications of Molecular Simulation in the Gas Industry: Monte Carlo Methods*, Editions Technip - IFP Publications, Paris, 2005.

48 P. Ungerer, C. Beauvais, J. Delhommelle, A. Boutin, B. Rousseau and A. H. Fuchs, Optimization of the anisotropic united atoms intermolecular potential for n -alkanes, *J. Chem. Phys.*, 2000, **112**, 5499–5510.

49 E. Bourasseau, P. Ungerer and A. Boutin, Prediction of Equilibrium Properties of Cyclic Alkanes by Monte Carlo

Open Access Article. Published on 21 October 2021. Downloaded on 2/2/2022 7:01:03 PM.
This article is licensed under a Creative Commons Attribution-NonCommercial 3.0 Unported Licence.



Simulation New Anisotropic United Atoms Intermolecular Potential New Transfer Bias Method, *J. Phys. Chem. B*, 2002, **106**, 5483–5491.

50 P. Pascual, P. Ungerer, B. Tavitian, P. Pernot and A. Boutin, Development of a transferable guest–host force field for adsorption of hydrocarbons in zeolites, *Phys. Chem. Chem. Phys.*, 2003, **5**, 3684–3693.

51 A. Schneider, R. W. Warren and E. J. Janoski, Formation of Perhydrophenalenes and Polyalkyladamantanes by Isomerization of Tricyclic Perhydroaromatics, *J. Org. Chem.*, 1966, **31**, 1617–1625.

52 B. Smit and T. L. M. Maesen, Towards a molecular understanding of shape selectivity, *Nature*, 2008, **451**, 671–678.

53 P. Bai, M. Y. Jeon, L. Ren, C. Knight, M. W. Deem, M. Tsapatsis and J. I. Siepmann, Discovery of optimal zeolites for challenging separations and chemical transformations using predictive materials modeling, *Nat. Commun.*, 2015, **6**, 5912.

54 C. Chizallet, Toward the Atomic Scale Simulation of Intricate Acidic Aluminosilicate Catalysts, *ACS Catal.*, 2020, **10**, 5579–5601.

55 P. S. F. Mendes, J. M. Silva, M. F. Ribeiro, P. Duchêne, A. Daudin and C. Bouchy, Quantification of metal-acid balance in hydroisomerization catalysts, *AIChE J.*, 2017, **63**, 2864–2875.

56 M. A. McKervey, Adamantane rearrangements, *Chem. Soc. Rev.*, 1974, **3**, 479.

57 L. Rollmann, L. A. Green, R. A. Bradway and H. K. C. Timken, Adamantanes from petroleum with zeolites, *Catal. Today*, 1996, **31**, 163–169.

58 L. Treps, A. Gomez, T. D. Bruin and C. Chizallet, Environment, Stability and Acidity of External Surface Sites of Silicalite-1 and ZSM-5 Micro and Nano Slabs, Sheets, and Crystals, *ACS Catal.*, 2020, **10**, 3297–3312.

59 G. Noh, Z. Shi, S. I. Zones and E. Iglesia, Isomerization and β-scission reactions of alkanes on bifunctional metal-acid catalysts, *J. Catal.*, 2018, **368**, 389–410.

60 P. Agarwal, M. Sahasrabudhe, S. Khandalkar, C. Saravanan and M. T. Klein, Molecular-Level Kinetic Modeling of a Real Vacuum Gas Oil Hydroprocessing Refinery System, *Energy Fuels*, 2019, **33**, 10143–10158.

61 B. E. Browning, I. Pitault, F. Couenne and M. Tayakout-Fayolle, Effects of Bifunctional Catalyst Geometry on Vacuum Gas Oil Hydrocracking Conversion and Selectivity for Middle Distillate, *Ind. Eng. Chem. Res.*, 2018, **57**, 16579–16592.

 This journal is © The Royal Society of Chemistry 2021